PORTLAND PRESS

Clinical Science

ACCEPTED MANUSCRIPT

Dual effects of fructose on ChREBP and FoxO1/3α are responsible for AldoB upregulation and vascular remodeling

Wei Cao, Tuanjie Chang, Xiao-qiang Li, Rui Wang, Lingyun Wu

Increased production of methylglyoxal (MG) in vascular tissues is one of the causative factors for vascular remodeling in different subtypes of metabolic syndrome, including hypertension and insulin resistance. Fructose-induced upregulation of aldolase B (AldoB) contributes to increased vascular MG production but the underlying mechanisms have been unclear. Serum levels of MG and fructose were determined in diabetic patients with hypertension. MG level had significant positive correlations with blood pressure and fructose level respectively. C57Bl/6 mice were fed with control or fructose-enriched diet for 3 months and ultrasonographic and histologic analyses were performed to evaluate arterial structural changes. Fructose-fed mice exhibited hypertension and high levels of serum methylglyoxal with normal glucose level. Fructose intake increased blood vessel wall thickness and vascular smooth muscle cell (VSMC) proliferation. Western blotting and real-time PCR analysis revealed that AldoB level was significantly increased in both the aorta of fructose-fed mice and the fructose-treated VSMCs, whereas AldoA expression was not changed. The knockdown of *AldoB* expression prevented fructose-induced MG overproduction and VSMC proliferation. Moreover, fructose significantly increased ChREBP, phosphorylated FoxO1/3α and Akt1 levels. Fructose induced translocation of ChREBP from the cytosol to nucleus and activated *AldoB* gene expression, which was inhibited by the knockdown of ChREBP. Meanwhile, fructose caused FoxO1/3α shuttling from the nucleus to cytosol and inhibited its binding to *AldoB* promoter region. Fructose-induced AldoB upregulation was suppressed by Akt1 inhibitor but enhanced by FoxO1/3α siRNA. Collectively, fructose activates ChREBP and inactivates FoxO1/3α pathways to upregulate AldoB expression and MG production, leading to vascular remodeling.

Cite as Clinical Science (2016) DOI: 10.1042/CS20160251

Dual effects of fructose on ChREBP and FoxO1/3α are responsible for AldoB upregulation and vascular remodeling

Wei Cao[1,2], Tuanjie Chang[3] , Xiao-qiang Li[4], Rui Wang[5,6,7], Lingyun Wu[1,6,8]*

[1] Department of Health Sciences, Lakehead University, Thunder Bay, Canada6

[2] School of Chemistry & Pharmacy, Northwest A&F University, Yangling, China

[3] Thunder Bay Regional Research Institute, Thunder Bay, Canada

[4] Department of Pharmacology, School of Pharmacy, Fourth Military Medical University, Xi'an, 710032, China

[5] Cardiovascular and Metabolic Research Unit, Lakehead University, Thunder Bay, Canada

[6] Cardiovascular and Metabolic Research Unit, Laurentian University, Canada

[7] Department of Biology, Laurentian University, Canada

[8] Health Sciences North Research Institute, Sudbury, Canada

*Correspondence: Lingyun Wu (lwu@lakeheadu.ca)

Short title: AldoB and vascular remodeling

Abstract

Increased production of methylglyoxal (MG) in vascular tissues is one of the causative factors for vascular remodeling in different subtypes of metabolic syndrome, including hypertension and insulin resistance. Fructose-induced upregulation of aldolase B (AldoB) contributes to increased vascular MG production but the underlying mechanisms have been unclear. Serum levels of MG and fructose were determined in diabetic patients with hypertension. MG level had significant positive correlations with blood pressure and fructose level respectively. C57Bl/6 mice were fed with control or fructose-enriched diet for 3 months and ultrasonographic and histologic analyses were performed to evaluate arterial structural changes. Fructose-fed mice exhibited hypertension and high levels of serum methylglyoxal with normal glucose level. Fructose intake increased blood vessel wall thickness and vascular smooth muscle cell (VSMC) proliferation. Western blotting and real-time PCR analysis revealed that AldoB level was significantly increased in both the aorta of fructose-fed mice and the fructose-treated VSMCs, whereas AldoA expression was not changed. The knockdown of *AldoB* expression prevented fructose-induced MG overproduction and VSMC proliferation. Moreover, fructose significantly increased ChREBP, phosphorylated FoxO1/3α and Akt1 levels. Fructose induced translocation of ChREBP from the cytosol to nucleus and activated *AldoB* gene expression, which was inhibited by the knockdown of ChREBP. Meanwhile, fructose caused FoxO1/3α shuttling from the nucleus to cytosol and inhibited its binding to *AldoB* promoter region. Fructose-induced AldoB upregulation was suppressed by Akt1 inhibitor but enhanced by FoxO1/3α siRNA. Collectively, fructose activates ChREBP and inactivates FoxO1/3α pathways to upregulate AldoB expression and MG production, leading to vascular remodeling.

Keywords Aldolase B, ChREBP, FoxO1/3α, Fructose, Hypertension.

Abbreviations:

AA, abdominal aorta; AGEs, advanced glycation endproducts; AldoB, aldolase B, CA, carotid artery; ChIP, chromatin immunoprecipitation; ChoRE, carbohydrate-responsive element; ChREBP, carbohydrate-responsive element-binding protein; DBP, diastolic blood pressure; DHAP, dihydroxyacetone phosphate; EDV, end-diastolic velocity; FoxO, forkhead box transcription factor of the O class; GLUT5, glucose transporter 5; GA3P, glyceraldehyde-3-phosphate; HR, heart rate; MA, mesenteric artery; MG, methylglyoxal; PSV, peak systolic velocity; RI, resistance index; SBP, systolic blood pressure; T2DM, type 2 diabetes mellitus; TSS, transcription start site; VSMC, vascular smooth muscle cell.

Introduction

High intake of fructose, primarily in the form of added dietary sugars, is increasingly recognized as one risk factor for the development of hypertension and diabetes [1,2]. Previous studies have shown that high fructose intake induces cardiovascular dysfunction in both animals and humans [3]. Epidemiologic data showed that adults taking high-fructose diets are more prone to atherosclerosis and vascular changes than those having normal diets [4]. Our previous animal studies linked fructose consumption to increased methylglyoxal (MG) production [5,6]. MG is one of the causative factors for hypertension and vascular complications of diabetes [7,8]. It can react with certain residues of proteins to form advanced glycation endproducts (AGEs) and cause the dysfunction of the modified proteins. MG is a highly reactive dicarbonyl metabolite produced during glucose and fructose metabolisms [5]. Fructose and MG levels in the blood or vascular tissues were elevated in animal metabolic syndrome models, such as spontaneously hypertensive rats [7], fructose-fed hypertensive rats [9], obese non-diabetic or diabetic Zucker rats [10].

Aldolase B (AldoB) is the key enzyme for the conversion of fructose to MG in vascular tissues [10,11]. Increased fructose level upregulates AldoB expression and results in increased MG production. However, the mechanisms by which fructose upregulates AldoB expression are not clear. As such, the strategies to intervene AldoB upregulation and MG overproduction during vascular remodeling remain elusive [12].

The carbohydrate-responsive element-binding protein (ChREBP) is a central transcription factor for the expression of key genes involved in energy metabolism after glucose intake [13, 14]. ChREBP can enter the nucleus and binds to carbohydrate-responsive element (ChoRE) core motifs [14]. Several ChoRE core motifs are found at the upstream of transcription start site (TSS) on *AldoB* promoter region and the binding of ChREBP to ChoRE after glucose induction was reported to upregulate hepatic *AldoB* gene expression [14,15]. Whether ChREBP regulates *AldoB* gene expression in VSMCs and whether the expression and activity (phosphorylation vs. dephosphorylation) of ChREBP in VSMCs are altered by fructose in hypertension or other forms of metabolic syndrome have been unknown. Furthermore, it has been reported that in cell survival signaling, the insulin-responsive phosphoinositide-3-kinase (PI3K)/Akt pathway mediates the proliferation of VSMCs [16]. Upon stimulation with growth factors, PI3K mediates the phosphorylation of Akt, which interacts with intracellular signaling molecules to promote cell survival. As prominent effectors of the PI3K/Akt pathway, the forkhead box transcription factor of the O class (FoxOs) is involved in diverse physiological functions, including apoptosis, cell proliferation, and metabolism [17]. The mammalian FoxO family contains four functional isoforms (FoxOl, 3α, 4, and 6). Among these, FoxO1 and 3α are abundantly expressed in blood

vessels and play an early role in the development of tissue insulin resistance [17]. It has been reported that insulin inhibits the activity of FoxO1/3α in blood vessels or VSMCs through Akt activation and leads to phosphorylation of FoxOs, and its binding to 14-3-3 proteins, and export to the cytoplasm [17-19]. Currently, there is no evidence for the regulation of *AldoB* gene expression by FoxOs in any tissue. Whether and how the interaction of fructose with FoxOs regulates *AldoB* gene expression in VSMCs have been unknown.

We hypothesized that fructose-induced overexpression of AldoB is mediated by FoxO1/3α and ChREBP. To test our hypothesis, mice were fed with a high-fructose diet to induce vascular remodeling. The changes in AldoB expression, the PI3K/Akt/FoxO pathway, and ChREBP signaling in VSMCs were analyzed. Our study provides the first evidence that fructose orchestrates the expression and activities of ChREBP and Akt1/FoxO pathways to upregulate AldoB expression and MG production, leading to vascular remodeling.

Materials and Methods

Diabetic mellitus patients with hypertension

The clinic study was conducted on hospitalized or ambulatory patients with type 2 diabetes mellitus (T2DM) at the Xijing hospital of the fourth military medical university (FMMU) in Xi'an, China. T2DM was diagnosed according to the criteria of the American Diabetes Association. At a regular ambulatory visit or at the time of hospitalization, participants underwent baseline anthropometric and physical exams. Blood samples were collected after 12 hour overnight fasting and separated serum samples were immediately stored at -80°C until analyzed for MG and fructose. Fasting blood glucose (FBG), total cholesterol (TC), high-density lipoprotein (HDL), low-density lipoprotein (LDL), triglyceride (TG) and glycosylated hemoglobin (HbA1c) levels were measured with standard laboratory techniques on a Hitachi 7600 Analyzer (Hitachi; reagents from Roche Diagnostics). Fasting insulin (FIns) was routinely measured using radioimmunoassay. Homeostasis model of insulin resistance (HOMA-IR) index was calculated according to the formula, HOMA-IR=FIns×FBG/22.5. For the purpose of research, we excluded patients who took anti-diabetic agents and those with acute or chronic infections, liver disease, autoimmune diseases and other serious concomitant diseases. The remaining patients with or without hypertension, aged 32 to 69 years old, were enrolled. Hypertension was diagnosed and categorized according to the guidelines of WHO [20]. We also recruited 26 healthy subjects with normal blood pressure and without diabetes from Xijing hospital (during their Annul physical exams), as the age- and sex-matched controls. The study protocol was approved by ethical committees of Xijing Hospital and FMMU, and informed consents were

obtained from all participants.

Animals and cell culture

All animal care and experimental procedures were approved by the Animal Care Committee of Lakehead University, following the guidelines of the Canadian Council on Animal Care. In-house-bred male C57BL/6 mice, 5 weeks old, were used. Prior to dietary manipulation, all mice were fed with standard rodent chow diet (Rodent RQ 22-5; Zelgler Bros Inc). The control mice were fed with the standard chow, while the experimental animals (body weight matched) were fed with a high fructose diet containing 60% fructose (wt/wt) (TD.89247; Harlan Laboratories Inc) for 12 weeks and allowed ad libitum access to water and food. Body weights of the mice were monitored monthly. In the final week of treatment, systolic blood pressure (SBP), diastolic blood pressure (DBP) and heart rate (HR) were measured using a non-invasive tail-cuff system (CODA-6, Kent Scientific). The mean of over six consecutive readings was used as the measurement of the blood pressure of each mouse. At the completion of the 12 week feeding period, echocardiographic and Doppler examination were performed. After the termination of the animals by inhalation of CO_2, tissues were taken and stored at -80°C. The blood was collected and serum separated by centrifugation.

To investigate whether the increase in blood vessel thickness and AldoB expression are due to an increase in blood pressure level or direct effects of fructose/MG on VSMCs, hypotensive drugs, nifedipine and Akt1 inhibitor, A674563 were administered daily by gavage to high fructose-fed mice. The control mice were fed with the standard chow. At the completion of the 2 week feeding period, SBP and DBP were measured using a non-invasive tail-cuff system. The animals were killed by inhalation of CO_2 and tissues were isolated as mentioned above.

Rat aortic VSMCs (A-10 line) from American Type Culture Collection were cultured in Dulbecco's modified Eagle's medium (DMEM) containing 10% fetal bovine serum (FBS) as described in our previous studies [21].

Primary rat aortic VSMCs were prepared from thoracic aorta of 2- to 3-month-old SD rats and assessed for purity as previously described [22]. The cells were maintained in DMEM supplemented with 10% FBS, 100 U/mL penicillin and 100 μg/mL streptomycin. The cells from passages 2-4 were used in experiments.

High frequency micro-ultrasound

Echocardiographic and Doppler examination were performed using a Vevo 2100 high-resolution ultrasound unit (Visualsonics). In brief, mice were fasted overnight and

anesthetized with 2-3.5% isoflurane initially and 1-2.5 % isoflurane during the entire procedure. The mice were laid on a temperature-controlled platform in the supine position with all legs taped to electrocardiogram electrodes for heart rate monitoring during the experiment. The left carotid artery (CA), abdominal aorta (AA), and superior mesenteric artery (MA) were imaged in the 2-dimensional short- and long-axis view, and time-varying tracings were recorded to examine vascular diameters and artery wall thickness. To determine blood flow velocity, the time-varying velocity waveforms were recorded in pulse-wave Doppler mode. Data were analyzed offline using the Vevo 2100 software (version 1.1.1, Visualsonics). From the M-mode recording, the wall thickness, end-diastolic and end-systolic internal dimensions were measured for three cardiac cycles and averaged. From Doppler spectra, the peak systolic velocity (PSV) and the end-diastolic velocity (EDV) were measured and averaged for 3 consecutive cardiac cycles. Resistance index (RI) as a measure of blood flow resistance in the downstream vasculature from where the sample volume was positioned, was calculated as RI = (PSV–EDV)/PSV.

Vascular morphology and smooth muscle cell counts

The CA at the carotid midsection, AA from the level of the diaphragm through to the superior mesenteric artery region, and MA near abdominal aorta were removed, fixed in 10% formalin solution, and embedded in paraffin. Sections (4 μm thick) were placed on glass slides, and paraffin was removed by xylene. Then, the tissue sections were stained with haematoxylin and eosin (H&E) reagent. Examination and photographs were taken with an IX70 inverted phase contrast microscope (Olympus).

For the quantification of smooth muscle cells, an anti-α-smooth muscle actin antibody was applied to formalin-fixed paraffin-embedded sections that had been previously subjected to antigen retrieval and blocked with 1% bovine serum albumin. The sections were stained with fluorescein isothiocyanate (FITC)-conjugated goat anti-rabbit immunoglobulin G (IgG) and counterstained with 4',6-diamidino-2-phenylindole (DAPI). Images were captured and the high-contrast image of DAPI-stained nuclei was overlaid with the α-smooth muscle actin-positive FITC-stained image (VSMCs). The total numbers of VSMCs per tissue sample was calculated by point counting the DAPI-stained nuclei in colocalized areas of FITC and DAPI as described [23]. Nuclei that did not colocalize with FITC were defined as other cell types (endothelial cells, fibroblasts, etc.). The vessel wall thicknesses were measured using mage-pro plus software (Media Cybernetics, Bethesda, MD, USA). Each data point represents at least 18 images from six animals.

Immunofluorescence microscopy

The expression of ChREBP, FoxO1, FoxO3α and AldoB on vascular tissues was assessed by immunohistochemistry performed on frozen sections. Briefly, the frozen sections were rehydrated in PBS for 5 min, permeabilized with 0.1% Triton X-100 and blocked with 10% goat serum. The sections were incubated overnight at 4°C with rabbit polyclonal anti-ChREBP antibody (NB400-135, Novus), anti-FoxO1(Cell Signaling), anti-FoxO3α (Cell Signaling) and mouse polyclonal anti-AldoB antibody (ab129728, Abcam). The sections were washed three times with PBS and then incubated with Rhodamine- or FITC-conjugated secondary antibodies. After several washes in PBS and coverslipped with a DAPI mounting medium, the images were collected using fluorescent microscopy (IX70, Olympus). Image analysis was performed with Image pro plus 6.0 software (Media Cybernetics CO.) referencing the method introduced previously [24, 25]. In short, the mean pixel density was assessed for manually cropped areas of uniform intensity in the nucleus or cytoplasm. All digital photographs were taken and measured in the same parameter setting to insure these data were comparable. The VSMCs in two random 400× microscopic fields per slide were measured. The statistic evaluated was the average ratio of the cytoplasmic region intensity to the nuclear region intensity for each microscopic field. Each data point represents 12 images from six animals.

Cell proliferation assay

Cell proliferation was determined using the MTT and 5-bromo-2'-deoxyuridine (BrdU) assays, respectively. The MTT test which measures metabolic activity as an indirect marker of cell proliferation, was performed as previously described [26]. BrdU incorporation assay was also used to evaluate the mitotic cell duplication with BrdU proliferation assay kits, according to manufacturer's instructions (Calbiochem).

In situ cell proliferation analysis

Proliferation in regions of the blood vessels was assayed using BrdU incorporation as previously described [27]. Briefly, BrdU (100 mg/kg) was injected intraperitoneally into mice, and 4 h later the blood vessels were removed and frozen-sectioned into 10-μm sections. Following fixation and denaturized with 4 mol/L HCl, the sections were immunostained with anti-BrdU antibody (Abcam). Immunofluorescence images were obtained using a confocal microscope (FV1000, Olympus, Japan).

siRNA transfection

A-10 cells were transfected with specific siRNAs to knock down the expression of *AldoA*, *AldoB, ChREBP, FoxO1*, and *FoxO3a* genes, using the DharmaFECT 2 reagent (Dharmacon) according to manufacturer's protocol. Non-targeting control siRNA was used as a transfection control. Briefly, the cells were starved for 24 h, and mixture of 100 nM siRNA and transfection reagent in serum-free DMEM were added to the culture medium. After 18 h of incubation, the transfection medium was replaced by DMEM containing 10% FBS. After exposure to different treatments, protein levels were determined by Western blotting and experiments were performed following 72 h exposure to siRNA.

Western blotting

After different treatments, total proteins of aortas from mice or A-10 cells were extracted with RIPA buffer containing protease inhibitor cocktail (Sigma). Nuclear and cytoplasmic extracts were prepared using the NE-PER nuclear and cytoplasmic extraction reagent kit (Pierce), and immunoblotting was performed as previously described [10]. Extracted proteins were quantified using the Bradford assay (Thermo Fisher). Equal amounts of proteins were denatured and separated by SDS-PAGE and transferred to nitrocellulose membranes for Western blot analysis using primary antibodies as follows: anti-AldoA (1:200; Santa Cruz Biotechnology), anti-AldoB (1:1000; Epitomics), anti-phospho-Akt1(Ser^{473}) (1:1000; Cell Signaling), anti-Akt1(1:1000; Cell Signaling), anti-ChREBP (1:1000; Novus), anti-FoxO1(1:1000; Cell Signaling), anti-FoxO3α (1:1000; Cell Signaling), anti-phospho-FoxO1(Ser^{256})(1:1000; Cell Signaling), anti-phospho-FoxO1 (Thr^{24})(1:1000; Cell Signaling), anti-phospho-FoxO3α (Ser^{256})(1:1000; Cell Signaling) and anti-β-actin (1:5000; Sigma). The immunoreactions were visualized by ECL detection Kit (GE Healthcare Life sciences) and exposed to x-ray films. Films of Western blots were scanned and quantified using an image processor program.

Real-time PCR

AldoB and AldoA mRNA was determined by a real-time PCR assay as previously described [10]. Briefly, total RNA was extracted from aorta tissues or A-10 cells using RNeasy Mini Kits (Qiagen) according to manufacturer's protocol. Total RNA was converted to cDNA using an iScript^{TM} cDNA Synthesis Kit (Bio-Rad). Real-time PCR was performed using SYBR Green PCR Master Mix (Bio-Rad) according to a two-step PCR protocol (1 min at 95°C, 40 cycles for 15 s at 95°C, 15 s at 60°C and 45 s at 72°C) with the iCycler iQ real-Time PCR Detection System (Bio-Rad). Each sample was run and analyzed in triplicate, and the mRNA level of AldoA or AldoB was normalized using β-actin as an internal control.

ChIP

ChIP assay was performed using Epi Tect ChIP One-Day Kit (Qiagen) according to manufacturer's protocol. Briefly, A-10 cells were cross-linked with 1% formaldehyde at 37°C for 10 min, stopped by the addition of glycine. The cells were sonicated to shear DNA to sizes between 500 to 1500 bp in sonication buffer. The sonicated supernatant (termed input) were immunoprecipitated with nonspecific rabbit IgG (the negative control), anti-ChREBP (NB400-135; Novus), anti-FoxO1 (ab39670; Abcam), anti-FoxO3α (ab12162; Abcam) or anti-Histone H3 (the positive control; ab8580; Abcam) antibodies. After purified, chromatin DNAs were analyzed by real-time PCR using EpiTect ChIP qPCR primers (Qiagen, GPR1075699(+)01A for FoxO1, GPR1075699(+)03A for FoxO3a, and GPR1075699(-)02A for ChREBP) targeting AldoB promoter region. A standard PCR program with 40 cycles was used. The binding intensity of ChREBP, FoxO1, or FoxO3α to the AldoB core promoter was normalized to the level of input using the same primers. A single PCR band was visualized by electrophoresis using 2% agarose gel stained with ethidium bromide.

Biochemical assay

Tissue samples were sonicated and centrifuged at 12000 g (10 min, 4°C). Total protein levels were determined using Coomassie plus assay reagent (Pierce). Glucose and fructose levels in serum and tissue samples were measured using a glucose assay kit (Bioassay Systems) and a fructose assay kit (Bioassay Systems) according to manufacturer's procedures, respectively. Insulin concentrations in serum samples were measured using a mouse insulin ELISA kit (Mercodia AB) according to manufacturer's procedures.

MG measurement

MG was measured with an *o*-phenylenediamine (*o*-PD)-based high-performance liquid chromatography assay as described before [10, 28, 29].

Chemicals

SH-6 (Akt Inhibitor III) was purchased from Calbiochem. Cell culture media, MG, D-fructose, insulin, BrdU and other chemicals were purchased from Sigma-Aldrich. Nifedipine and A674563 were purchased from Selleckchem.

Statistical analysis

All data are represented as mean ± S.E.. All the statistical analysis was performed using SPSS 16.0 (SPSS Inc., Chicago, IL, USA). Datasets were tested for normality using the Kolmogorov-Smirnov test before further analysis. Correlations were assessed using Pearson's correlation test. The independent determinants for hypertension were assessed by binary logistic regression analysis, and the covariates chosen to enter the multivariate analysis model included gender, age, smoke, serum glucose, MG and fructose levels. An unpaired two-tailed student's *t* test was used to compare data between two groups, whereas one-way ANOVA with Tukey's post-hoc tests was used for multiple comparisons. The difference between data was considered significant when *P* value was less than 0.05.

Results

Correlation of serum MG and fructose levels with hypertension in T2DM patients

Demographic and clinical characteristics of the diabetic patients and healthy volunteers (control) are shown in Supplementary Table S1. There were no statistically significant differences in age, sex, body mass index, high-density lipoprotein and low-density lipoprotein levels between the patients and control groups. Fasting serum glucose, insulin, HOMA insulin resistance index (HOMA-IR), total cholesterol, triglyceride and glycosylated hemoglobin levels were increased in the diabetic groups compared to control. Hypertensive patients had significantly higher serum MG (Figure 1A) and fructose (Figure 1B) concentrations than healthy subjects. In those diabetic patients with normal blood pressure, serum MG levels (Figure 1A) and fructose levels (Figure 1B) were already significantly elevated. Correlation analysis (Figure 1C) showed MG levels had a positive correlation with blood pressure. The correlation coefficients were 0.628 ($P < 0.001$, SBP) and 0.659 ($P < 0.001$, DBP) respectively using simple correlational analysis. The fructose levels were also positively correlation with SBP with the correlation coefficient of 0.377 ($P < 0.001$) and with DBP with the correlation coefficient of 0.474 ($P < 0.001$) (Figure 1D). Moreover, Correlation analysis (Figure 1E) showed MG levels had a significant positive serum fructose levels 0.759 ($P < 0.001$). Multivariate logistic regression analysis showed that the significant risk factors for hypertension included serum fructose (P=0.046), glucose (P=0.033) and MG (P=0.023) levels but not female gender (P=0.762), age > 60 years (P=0.061) and smoke (P=0.507) (Figure 1F).

Fructose-induced MG overproduction and hypertension

After a 12-week dietary intervention, fructose-fed mice had higher SBP and DBP than those with control diet ($P < 0.05$, Supplementary Table S2), whereas body weights and serum

glucose levels were similar for the two groups. Fructose-fed mice exhibited significantly higher serum levels of fructose, MG, insulin and HOMA-IR than in control mice. Similarly, fructose-fed mice had significantly elevated fructose and MG contents in their aortae in comparison to control mice without difference in aortic glucose levels (Supplementary Table S3).

Fructose-induced vascular remodeling

After a 12-week dietary intervention, color Doppler blood flow analysis on living animals revealed that the high-fructose diet significantly increased RI of CA, AA, and MA (Figure 2A and 2B-a). EDV in CA, AA, and MA of fructose-fed mice decreased by 58.5 %, 50.2 %, and 43.7 %, respectively, as the PSV showed only minimal changes (Figure 2A-b and Supplementary Figure S1). Thus, the increase in RI was directly related to a decreased EDV. As observed in the time-varying tracings of individual blood vessels, the wall thickness was significantly increased in CA, AA, and MA of fructose-fed mice relative to control mice (Figure 2A-c and B-b). Furthermore, the diastolic and systolic diameters of CA, AA, and MA of fructose-fed mice were significantly smaller than those of the control mice (Figure 2B-c and -d). These data demonstrated that the high-fructose diet induced vascular remodeling and decreased vascular compliance, likely due to medial hyperplasia.

Vascular morphology analysis on H&E stained histology sections showed increased blood vessel thickness in fructose-fed mice (Figure 3A). The accumulation of VSMCs in blood vessel wall was further identified by immunohistochemistry with the use of an anti-α-smooth muscle actin antibody (FITC staining) and DAPI to stain the nucleus. By co-localization of FITC and DAPI, we quantified the number of VSMCs within the vascular wall. The numbers of VSMCs per blood vessel were significantly increased in CA, AA, and MA from fructose-fed mice relative to control mice (23.1%, 29.9%, and 30.7% increase, respectively, $P < 0.05$) (Figure 3B). Moreover, the blood wall thickness of CA, AA, and MA of fructose-fed mice were significantly increased relative to control mice (Figure 3C).

Fructose-induced upregulation of AldoB, ChREBP, Akt1, and FoxOs

As shown in Figure 4A, aortic AldoB mRNA level of fructose-fed mice was increased by 86% in comparison with that of control mice. Western blotting analysis revealed that AldoB protein level was significantly increased in the aorta by 125% in the fructose-fed mice in comparison with that of control mice (Figure 4B).

Fructose-fed mice exhibited significantly increased ChREBP protein levels in their aortae (Figure 4C). The ratio of phosphorylated (inactivated) to total FoxO1 levels was 180% higher in

fructose-fed mice than control mice ($P < 0.05$, Figure 4D). Consistent with the increase in phosphorylated FoxO1, the ratios of phosphorylated FoxO3α to total FoxO3α proteins was also significantly increased in fructose-fed mice ($P < 0.05$, Figure 4D). Furthermore, fructose-fed mice exhibited 148% increase in the ratio of phosphorylated to total Akt1 protein ($P < 0.05$) (Figure 4E), indicative of increased activation of Akt1.

The mediation of fructose-induced MG overproduction and VSMC proliferation by AldoB expression

To clarify a regulatory role of AldoB in fructose-induced VSMC proliferation, we treated the cultured A-10 cells with fructose or fructose plus insulin. Fructose (0.01 to 10 mM) increased AldoB expression at the protein (Supplementary Figure S2A and B) and mRNA levels (Supplementary Figure S3A) in a concentration-dependent manner. In addition, fructose increased AldoB protein level in a time-dependent manner with a maximal effect observed at 6 and 12 hrs after treatment (Supplementary Figure S2B). Fructose treatment did not change AldoA expression at both the transcriptional and translational levels in A-10 cells (Supplementary Figure S2A and Supplementary Figure S3A). In contrast, insulin increased both *AldoA* and *AldoB* gene expression in A-10 cells to different degrees. We further tested the effects of fructose on cell proliferation using MTT assay. As shown in Supplementary Figure S3B, fructose increased the proliferation of A-10 cells in a time- and concentration-dependent manner.

We next investigated the effects of aldolase inhibition on fructose-stimulated VSMC proliferation. The expression of *AldoA* and *AldoB* in cultured A-10 cells was knocked down via transfection with AldoA and AldoB siRNAs (Figure 5A). Six-hour treatment of the cells with fructose and/or insulin increased the MG levels in control siRNA- or AldoA siRNA-transfected cells, but did not change the MG level in AldoB siRNA-transfected cells at all (Figure 5B). MTT assay results demonstrated that fructose and/or insulin increased the proliferation of A-10 cells by 62.4 ± 14.2% and 84.6 ± 20.4%, respectively. AldoB siRNA, but not AldoA siRNA, significantly inhibited the cell proliferation induced by fructose and/or insulin ($P < 0.05$) (Figure 5C). Similar results were obtained using BrdU assays (Supplementary Figure S4). These data suggest that AldoB, not AldoA, plays a key role in vascular MG overproduction and VSMC proliferation.

Fructose-induced intracellular ChREBP shuttling

To explore the mechanisms for fructose-induced upregulation of AldoB in VMSCs, we examined ChREBP expression in A-10 cells. ChREBP expression was markedly increased in VSMCs by fructose and/or insulin stimulation (Figure 6A). Translocation of ChREBP to the

nucleus marks the activation of cells [14]. In our study, ChREBP proteins were detected in the nuclei of A-10 cells at a marginal level, but its expression in the cytosol was abundant under resting conditions (Figure 6B). Fructose and/or insulin stimulated more ChREBP translocation to the nucleus.

To determine the binding of ChREBP to AldoB promoter, ChIP assays were performed. *AldoB* PCR products were only detected in the samples immunoprecipitated with anti-ChREBP, but not in those immunoprecipitated with non-immune serum (Figure 6C). These findings suggest that ChREBP binds to *AldoB* gene and that fructose was capable of increasing the ChREBP-stimulated *AldoB* promoter activity. Insulin had a similar effect as that of fructose, enhancing ChREBP-stimulated *AldoB* promoter activity by approximately 80% (Figure 6C).

Consistent with our results from cultured A-10 cells, ChREBP expression, detected by immunocytochemical analysis, was predominantly located in the cytoplasm of aortic tissues from control mice, whereas the aortae of fructose-fed mice showed a marked increase in ChREBP expression in the nucleus (Figure 6D). Compared to the cytoplasmic/nuclear ratio of ChREBP (1.63±0.17) in control group, the ratio in fructose-fed group was significantly decreased to 1.02± 0.06.

The role of ChREBP in the regulation of AldoB expression

AldoB expression in aortic tissues from fructose-fed mice was obviously increased compared with that of control mice. Merging of AldoB and ChREBP labeling showed an increased interaction between AldoB and ChREBP in the fructose diet group, which was localized primarily in the nucleus (Figure 6D).

ChREBP-siRNA treatment decreased ChREBP protein level in A-10 cells by approximately 49.8% (Figure 7A). Fructose and/or insulin increased AldoB expression, which was significantly inhibited by ChREBP-siRNA. The basal level of AldoB proteins in A-10 cells was also downregulated by ChREBP-siRNA (Figure 7A). Similarly, ChREBP knockdown decreased MG production and cell proliferation in A-10 cells in the absence and presence of fructose and/or insulin treatment (Figure 7B and C). Taken together, these data suggest that AldoB expression and the related MG production are significantly regulated by ChREBP.

The relationship between Akt1-FoxO pathway and AldoB expression

Akt1 and its downstream targets, FoxO1 and Fox3α, are involved in fructose-induced vascular remodeling. In fructose and/or insulin-treated A-10 cells, the levels of phosphorylated Akt1, FoxO1, and FoxO3α proteins were significantly increased (Supplementary Figure S5A).

The inhibition of Akt1 activity with SH-6 dramatically decreased Akt1 phosphorylation, but not total Akt1 protein level. SH-6 also inhibited FoxO1and FoxO3α phosphorylation in A-10 cells with or without fructose and/or insulin treatment. Moreover, fructose-induced AldoB upregulation was markedly suppressed by SH-6. This effect was more pronounced than that in insulin-treated cells (Supplementary Figure S5A).

Supplementary Figure S5B-C showed that fructose- and/or insulin-induced MG production and cell proliferation were markedly suppressed by SH-6, similar to the effect of ChREBP siRNA.

Fructose-induced intracellular FoxO1/3α shuttling and upregulation of *AldoB* gene

FoxO1/3α proteins resided primarily in the nucleus of A-10 cells (Figure 8A). When stimulated by fructose and/or insulin, both FoxO1 and FoxO3α shuttled from the nucleus to cytoplasm, evidenced by decreased cytosolic and increased nuclear levels of FoxO1/3α observed. The immunocytochemical analysis (Supplementary Figure S6) also confirmed the marked increase of FoxO1/3α in the cytoplasm of aortic tissues from fructose-fed mice. To investigate whether *AldoB* promoter is a binding target of FoxO1 and FoxO3α, we performed ChIP assays in the presence or absence of fructose and/or insulin. As shown in Figure 8B, there were obvious PCR products in FoxO1 and FoxO3α immunoprecipitates using AldoB primers, but no PCR product was obtained in normal rabbit IgG immunoprecipitates. These data showed that FoxO1/3α bind to the *AldoB* promoter DNA in A-10 cells. In addition, FoxO1/3α recruitment to the *AldoB* promoter was significantly decreased after fructose and/or insulin treatment. Remarkably, the levels of FoxO1 binding to *AldoB* promoter were decreased to 66% and 67% of the quiescent levels after fructose and insulin treatment, respectively (Figure 8B). Similar to FoxO1, a significant decrease in the levels of FoxO3α binding to *AldoB* promoter was observed after the treatment with fructose and/or insulin.

We also measured AldoB protein levels in A-10 cells following knockdown of FoxO1 and FoxO3α expression with the respective siRNA (Figure 8C and D). FoxO1 and FoxO3α knockdown augmented AldoB expression in unstimulated A-10 cells by approximately 31.7% and 44.4%, respectively. In addition, fructose and/or insulin-induced upregulation of AldoB proteins was markedly enhanced by FoxO1/3α siRNA.

Discussion

Metabolic syndrome is a cluster of metabolic abnormalities associated with type 2 diabetes, obesity, and hypertension, including hyperglycemia, glucose intolerance, insulin resistance,

dyslipidaemia, and high blood pressure, respectively [30]. As early as in the 1950s, it was recognized that high-sucrose diets rapidly induced features of metabolic syndrome in animals, including hypertension, insulin resistance, hyperlipidemia and hyperuricemia [31]. Further studies demonstrated that when rats were pair-fed with equivalent amounts of fructose and glucose, only the fructose-fed rats developed symptoms of metabolic syndrome [32-34]. Human body handles glucose and fructose in different ways. Fructose is absorbed in the intestine via specific transporters, primarily glucose transporter 5 (GLUT5). Although fasting serum concentrations of fructose are low (10−60 μM), its postprandial concentrations may reach 1 mM systemically in healthy people and 2.2 mM in patients with diabetes [33, 35, 36]. The liver metabolizes at least half of fructose [37], and adipose and vascular tissues also participate in local metabolic disposal of fructose [33, 38]. In the cytosol, glucose is metabolized through the glycolytic pathway into fructose-1,6-diphosphate [39], which subsequently forms glyceraldehyde-3-phosphate (GA3P) and dihydroxyacetone phosphate (DHAP), catalyzed by AldoA [40, 41]. On the other hand, fructose can be rapidly phosphorylated by fructokinase to fructose-1-phosphate, which is cleaved by rate-limiting AldoB to generate GA3P and DHAP. The latters are finally non-enzymatically converted to MG [10, 41]. AldoB is a key enzyme for the conversion of fructose to MG [10, 11], whereas AldoA regulates the conversion of glucose to MG.

MG is a known risk factor for hypertension and diabetes [7,42,43]. Increased MG levels were observed in diabetes patients [8,44] and in the aorta, kidney, and retina of hypertensive or diabetic animals [6,10,11,28,45,46]. Because high levels of glucose activate the polyol pathway and enhanced fructose production in diabetic states, so MG is mainly generated either through fructose metabolized from glucose by the polyol pathway or derived from the diet directly in formation under conditions of hyperglycemia, diabetes mellitus and its complications. Moreover, our previous experiments demonstrated that elevated MG levels were also presented in the metabolic syndrome without hyperglycaemia, such as in hypertension [9]. The MG levels in plasma and aorta were increased in spontaneously hypertensive rats (SHRs), although no difference in blood glucose levels between SHRs and control rats [46]. Chronic treatment with an AGE inhibitor, aminoguanidine attenuated blood pressure increase in SHRs [47]. So the MG MG-induced AGEs contribute to the pathogenesis of hypertension. In the current study, we further verified that fructose and MG levels are positively correlated with blood pressure in diabetic patients. The significant risk factors for hypertension included serum fructose, glucose and MG levels. A causative relationship between fructose-induced MG overproduction and hypertension is thus suggested in a clinical setting.

AldoB is a major enzyme responsible for high fructose-induced MG overproduction in endothelial cells and VSMCs [10,11,21,48]. Altered cardiovascular and metabolic functions in high-fructose fed animals are similar to metabolic syndrome of humans [49]. Our present study used the mice fed chronically with a fructose-rich diet to investigate the development of vascular remodeling and hypertension. We found that fructose-fed mice exhibited hypertension, increased MG production, and AldoB over-expression in vascular tissues. Vascular remodeling in these animals is manifested with decreased lumen diameter and increased wall thickness in different blood vessel walls (Figure 2). Arterial stiffness has been routinely reported in both animal models of metabolic syndrome and patients [50]. To this end, our ultrasonographic imaging analysis on living animals showed increased RI of the arteries in fructose-fed mice, indicating increased wall stiffness and the increased downstream circulatory resistance [51].

The mechanisms for fructose-induced upregulation of AldoB expression are the activation of ChREBP and inactivation of FoxO1/3α. ChREBP is expressed in numerous tissues, including skeletal muscle, heart, pancreatic islet, kidney, liver, fat, and VSMCs [14,52,53]. It was shown previously that phosphorylated and inactivated ChREBP could be dephosphorylated and activated by glucose. The activated ChREBP then enters the nucleus and binds to ChoRE core motifs (CACGTG) present in the promoter region of carbohydrate-sensitive genes [14,15,52]. One of the consequences is the upregulation of *AldoB* gene expression [15]. Sprague-Dawley rats fed with a 63% fructose diet displayed an increased nuclear distribution of ChREBP protein in the liver [54]. Although we did not measure the level of phosphorylated ChREBP proteins in VSMCs due to the unavailability of the specific anti-phosphorylated ChREBP antibody, our data showed that fructose feeding significantly increased aortic levels of total ChREBP proteins in the mice (Figure 4) and that fructose treatment of cultured A-10 cells markedly increased ChREBP shuttling from the cytoplasm to nucleus (Figure 6B). Using the combination of ChIP and Q-PCR techniques, we detected an increased binding of ChREBP to *AldoB* promoter region in fructose-tread A-10 cells (Figure 6C). Specific knockdown of ChREBP expression prevented fructose-induced AldoB expression, MG overproduction, and proliferation of A-10 cells (Figure 7). It is clear that ChREBP plays an important role in the regulation of *AldoB* expression and related MG production in VSMCs.

Phosphorylated FoxO is transcriptionally inactive and dephosphorylated FoxO is transcriptionally active. Once phosphorylated, FoxOs cannot bind to or will be dissociated from the promoter region of its target genes since it will be either retained in the cytosol or exported from the nucleus to cytosol [17]. Our studies demonstrated that the fructose-fed mice exhibited significantly higher levels of phosphorylated FoxO1 and FoxO3α in vascular tissues (Figure 4)

and the levels of phosphorylated FoxO1 and phosphorylated FoxO3α were significantly increased after fructose stimulation in VSMCs (Supplementary Figure 5). When stimulated by fructose, both FoxO1 and FoxO3α shuttled from the nucleus to cytoplasm (Figure 8A). FoxO1/3α can bind to the chromatinized *AldoB* promoter DNA in A-10 cells. This binding was significantly decreased after fructose and/or insulin treatment (Figure 8B). Furthermore, specific knockdown of FoxO1/3α increased AldoB expression in VSMCs with or without the treatment with fructose and/or insulin (Figure 8C-D). All these data support our hypothesis that the binding sites for FoxO1/3α are located downstream of the TSS of the *AldoB* promoter region (http://www.sabiosciences.com/chipqpcrsearch.php?species_id=1&factor=FOXO1&gene=ALDOB). The binding of FoxO1 and/or FoxO3α to the promoter region blocks *AldoB* gene transcription. FoxO1 and FoxO3α are likely the negative regulators of AldoB mRNA transcription. Fructose treatment increased phosphorylation and inactivation of FoxO1/3α, upregulating *AldoB* gene expression and MG overproduction. VSMC proliferation and vascular remodeling are the consequence of this chain reaction.

Our previous studies showed an increased Akt1 activity in aortic tissues of rats with metabolic syndrome [55]. In the present study, we found that knockdown of FoxO1/3α or inhibition of Akt activity prevented fructose-induced AldoB expression. In the presence of Akt inhibitor, fructose-induced phosphorylation of FoxO1/3α was significantly reduced, suggesting that Akt1 likely mediates the activation of FoxOs in VSMCs. Similar results were obtained in primary culture of vascular smooth muscle cells (Supplementary Figure S7).

In our previous animal observation and the data reported by others [56], the blood pressure in male C57BL/6 mice was significantly increased after 2 weeks of high fructose ingestion. To investigate whether the increase in blood vessel thickness and AldoB expression are due to an increase in blood pressure level or the direct effects of fructose or MG on VSMCs, hypotensive drug, nifedipine, and normal saline (vehicle) were administered daily by gavage to high fructose-fed mice for 14 days. Moreover, to confirm the role of Akt1 on AldoB upregulation and vascular remodeling *in vivo*, the high-fructose-fed mice were also treated with Akt1 inhibitor, A674563. The SBP, DBP, fructose, insulin and MG in mice were moderately increased on day 14 of high fructose ingestion, and nifedipine could decrease blood pressure, but there was no significant difference in other systemic characteristics among vehicle, nifedipine and A674563 treated groups (Supplementary Table S4 and S5). Microscopic examination revealed that the wall thickness was significantly increased in MA of fructose-fed mice relative to the control mice. Nifedipine could not significantly inhibit the vascular hyperplasia induced by high fructose, whereas Akt1 inhibitor markedly reduced MA wall thickness relative to fructose-fed mice almost without

lowering blood pressure (Supplementary Figure S8).

We also explored the effect of nifedipine and Akt1 inhibitor on in situ proliferation of VSMCs using BrdU assay. As showed in Supplementary Figure S9, Akt1 inhibitor-treated mice exhibited less proliferation of VSMCs in CA, AA and MA compared with vehicle-treated mice ($P < 0.01$), suggesting that activation of Akt1 signaling substantially contributes to enhanced proliferation of VSMCs at the early phase of fructose-induced arterial remodeling. However, there was no significant difference in the proliferation of VSMCs between nifedipine and vehicle-treated model groups. These data further confirmed that the vascular remodeling was directly related to fructose on VSMCs. Similar to the results of VSMCs *in vitro*, AldoB expression in aortas was down-regulated and FoxO1/3α expression in nuclear were increased when the fructose-fed mice were administrated with Akt1 inhibitor (Supplementary Figure S10). Akt1 inhibitor had no obvious effect on the fructose-induced increment of ChREBP expression. On the other hand, the expressions of AldoB and ChREBP and the nucleocytoplasmic distribution of FoxO1 and FoxO3α were not changed after administration of nifedipine in fructose-fed mice. These findings indicate that Akt1 can mediate, at least in part, fructose-induced up-regulation of AldoB in aortas.

In conclusion, fructose-induced vascular remodeling and development of hypertension are largely mediated by the upregulation of AldoB in vascular SMCs. Fructose-upregulated AldoB expression promotes the conversion of fructose to MG, both contributing to VSMC proliferation and vascular remodeling in hypertension. The mechanisms for fructose-induced upregulation of AldoB expression are the activation of ChREBP and Akt1-mediated inactivation of FoxO1/3α in VSMCs (Supplementary Figure S11). ChREBP and FoxO1/3a may serve as novel therapeutic targets for the prevention and treatment of fructose-induced vascular remodeling in metabolic syndrome.

Acknowledgements

We are grateful to Dr. Quihui Cao for her technical assistance and to Dr. Sarathi Mani and Ms. Ashley Untereiner for their assistance in the ultrasound biomicroscopy analysis. We acknowledge Dr. Wensheng Chen, Ms. Xiangying Feng, and Dr. Maigui Yang at Xijing Hospital for their help in collecting hypertensive patient data.

Funding

This research has been supported by a Grant-in-aid from the Heart and Stroke Foundation of Canada and Heart and Stroke Foundation-Ontario Mid-Career Investigator Award to LW.

Author Contribution

Wei Cao designed the study, performed the experiments and data analysis, prepared the figures, and drafted the manuscript. Tuanjie Chang designed the cell study and contributed to the writing of the manuscript. Xiao-qiang Li designed the human study, performed the experiments, and analyzed the data. Rui Wang edited and revised the manuscript, contributed to discussion, and interpreted the results of the experiments. Lingyun Wu developed the overall research plan, contributed to analysis and interpretation, and reviewed and edited the manuscript. Lingyun Wu is the guarantor of this work and, as such, had full access to all the data in the study and takes responsibility for the integrity of the data and the accuracy of the data analysis.

References

1. Ha, V., Jayalath, V.H., Cozma, A.I., Mirrahimi, A., de Souza, R.J. and Sievenpiper, J.L. (2013) Fructose-containing sugars, blood pressure, and cardiometabolic risk: A critical review. Curr. Hypertens. Rep. **15**, 281-297
2. Dhingra, R., Sullivan, L., Jacques, P.F., Wang, T.J., Fox, C.S., Meigs, J.B., D'Agostino, R.B., Gaziano, J.M. and Vasan, R.S. (2007) Soft drink consumption and risk of developing cardiometabolic risk factors and the metabolic syndrome in middle-aged adults in the community. Circulation **116**, 480-488
3. Malik, V.S., Popkin, B.M., Bray, G.A., Despres, J.P. and Hu, F.B. (2010) Sugar-sweetened beverages, obesity, type 2 diabetes mellitus, and cardiovascular disease risk. Circulation **121**, 1356-1364
4. Johnson, R.J., Segal, M.S., Sautin, Y., Nakagawa, T., Feig, D.I., Kang, D.H., Gersch, M.S., Benner, S. and Sanchez-Lozada, L.G. (2007) Potential role of sugar (fructose) in the epidemic of hypertension, obesity and the metabolic syndrome, diabetes, kidney disease, and cardiovascular disease. Am. J. Clin. Nutr. **86**, 899-906
5. Desai, K. and Wu, L. (2007) Methylglyoxal and advanced glycation endproducts: New therapeutic horizons? Recent Pat. Cardiovasc. Drug Discov. **2**, 89-99
6. Wu, L. and Juurlink, B.H. (2002) Increased methylglyoxal and oxidative stress in hypertensive rat vascular smooth muscle cells. Hypertension **39**, 809-814
7. Wang, X., Desai, K., Chang, T. and Wu, L. (2005) Vascular methylglyoxal metabolism and the development of hypertension. J. Hypertens. **23**, 1565-1573
8. Wang, H., Meng, Q.H., Gordon, J.R., Khandwala, H. and Wu, L. (2007) Proinflammatory and proapoptotic effects of methylglyoxal on neutrophils from patients with type 2 diabetes mellitus. Clin. Biochem. **40**, 1232-1239
9. Wang, X., Jia, X., Chang, T., Desai, K. and Wu, L. (2008) Attenuation of hypertension development by scavenging methylglyoxal in fructose-treated rats. J. Hypertens. **26**, 765-772
10. Liu, J., Wang, R., Desai, K. and Wu, L. (2011) Upregulation of aldolase b and overproduction of methylglyoxal in vascular tissues from rats with metabolic syndrome. Cardiovasc. Res. **92**, 494-503
11. Liu, J., Mak, T.C., Banigesh, A., Desai, K., Wang, R. and Wu, L. (2012) Aldolase b knockdown prevents high glucose-induced methylglyoxal overproduction and cellular dysfunction in endothelial cells. PloS One **7**, e41495
12. Alexander, M.R. and Owens, G.K. (2012) Epigenetic control of smooth muscle cell

differentiation and phenotypic switching in vascular development and disease. Annu. Rev. Physiol. **74**, 13-40

13. Dentin, R., Pegorier, J.P., Benhamed, F., Foufelle, F., Ferre, P., Fauveau, V., Magnuson, M.A., Girard, J. and Postic, C. (2004) Hepatic glucokinase is required for the synergistic action of chrebp and srebp-1c on glycolytic and lipogenic gene expression. J. Biol. Chem. **279**, 20314-20326
14. Ma, L., Robinson, L.N. and Towle, H.C. (2006) Chrebp*mlx is the principal mediator of glucose-induced gene expression in the liver. J. Biol. Chem. **281**, 28721-28730
15. Davies, M.N., O'Callaghan, B.L. and Towle, H.C. (2008) Glucose activates chrebp by increasing its rate of nuclear entry and relieving repression of its transcriptional activity. J. Biol. Chem. **283**, 24029-24038
16. Wang, C.C., Gurevich, I. and Draznin, B. (2003) Insulin affects vascular smooth muscle cell phenotype and migration via distinct signaling pathways. Diabetes **52**, 2562-2569
17. Accili, D. and Arden, K.C. (2004) Foxos at the crossroads of cellular metabolism, differentiation, and transformation. Cell **117**, 421-426
18. Allard, D., Figg, N., Bennett, M.R. and Littlewood, T.D. (2008) Akt regulates the survival of vascular smooth muscle cells via inhibition of foxo3a and gsk3. J. Biol. Chem. **283**, 19739-19747
19. Abid, M.R., Yano, K., Guo, S., Patel, V.I., Shrikhande, G., Spokes, K.C., Ferran, C. and Aird, W.C. (2005) Forkhead transcription factors inhibit vascular smooth muscle cell proliferation and neointimal hyperplasia. J. Biol. Chem. **280**, 29864-29873
20. Mancia, G., Fagard, R., Narkiewicz, K., Redon, J., Zanchetti, A., Bohm, M., Christiaens, T., Cifkova, R., De Backer, G., Dominiczak, A. et al. (2013) 2013 esh/esc guidelines for the management of arterial hypertension: The task force for the management of arterial hypertension of the european society of hypertension (esh) and of the european society of cardiology (esc). J. Hypertens. **31**, 1281-1357
21. Chang, T., Wang, R. and Wu, L. (2005) Methylglyoxal-induced nitric oxide and peroxynitrite production in vascular smooth muscle cells. Free Radic. Biol. Med. **38**, 286-293
22. Chen, Y.M., Wu, K.D., Tsai, T.J. and Hsieh, B.S. (1999) Pentoxifylline inhibits pdgf-induced proliferation of and tgf-beta-stimulated collagen synthesis by vascular smooth muscle cells. J. Mol. Cell Cardiol. **31**, 773-783
23. Banerjee, I., Fuseler, J.W., Price, R.L., Borg, T.K. and Baudino, T.A. (2007) Determination of cell types and numbers during cardiac development in the neonatal and adult rat and

mouse. Am. J. Physiol. Heart Circ. Physiol. **293**, H1883-1891

24. Soboleva, T.A., Jans, D.A., Johnson-Saliba, M. and Baker, R.T. (2005) Nuclear-cytoplasmic shuttling of the oncogenic mouse unp/usp4 deubiquitylating enzyme. J. Biol. Chem. **280**, 745-752
25. Wang, Y.E., Park, A., Lake, M., Pentecost, M., Torres, B., Yun, T.E., Wolf, M.C., Holbrook, M.R., Freiberg, A.N. and Lee, B. (2010) Ubiquitin-regulated nuclear-cytoplasmic trafficking of the nipah virus matrix protein is important for viral budding. PLoS Pathog. **6**, e1001186
26. Yang, G., Wu, L. and Wang, R. (2006) Pro-apoptotic effect of endogenous h2s on human aorta smooth muscle cells. FASEB J. **20**, 553-555
27. Qi, Y.X., Yao, Q.P., Huang, K., Shi, Q., Zhang, P., Wang, G.L., Han, Y., Bao, H., Wang, L., Li, H.P., et al. (2016) Nuclear envelope proteins modulate proliferation of vascular smooth muscle cells during cyclic stretch application. Proc. Natl. Acad. Sci. U S A. **113**, 5293-5298
28. Dhar A, Desai K, Kazachmov M, Yu P, Wu L. Methylglyoxal production in vascular smooth muscle cells from different metabolic precursors. *Metabolism: clinical and experimental*. 2008;57:1211-1220
29. Dhar, A., Desai, K., Kazachmov, M., Yu, P. and Wu, L. (2008) Methylglyoxal production in vascular smooth muscle cells from different metabolic precursors. Metabolism **57**, 1211-1220
30. Eckel, R. H., Grundy, S. M. and Zimmet, P. Z. (2005) The metabolic syndrome. Lancet **365**, 1415-1428
31. Portman, O.W., Lawry, E.Y. and Bruno, D. (1956) Effect of dietary carbohydrate on experimentally induced hypercholesteremia and hyperbetalipoproteinemia in rats. Proc. Soc. Exp. Biol. Med. **91**, 321-323
32. Gersch, M.S., Mu, W., Cirillo, P., Reungjui, S., Zhang, L., Roncal, C., Sautin, Y.Y., Johnson, R.J. and Nakagawa, T. (2007) Fructose, but not dextrose, accelerates the progression of chronic kidney disease. Am. J. Physiol. Renal. Physiol. **293**, F1256-1261
33. Johnson, R.J., Perez-Pozo, S.E., Sautin, Y.Y., Manitius, J., Sanchez-Lozada, L.G., Feig, D.I., Shafiu, M., Segal, M., Glassock, R.J., Shimada, M. et al. (2009) Hypothesis: Could excessive fructose intake and uric acid cause type 2 diabetes? Endocr. Rev. **30**, 96-116
34. Nakagawa, T., Hu, H., Zharikov, S., Tuttle, K.R., Short, R.A., Glushakova, O., Ouyang, X., Feig, D.I., Block, E.R., Herrera-Acosta, J. et al. (2006) A causal role for uric acid in fructose-induced metabolic syndrome. Am. J. Physiol. Renal. Physiol. **290**, F625-631
35. Mayes, P.A. (1993) Intermediary metabolism of fructose. Am. J. Clin. Nutr. **58**, 754S-765S
36. Kawasaki, T., Igarashi, K., Ogata, N., Oka, Y., Ichiyanagi, K., Yamanouchi, T. (2012)

Markedly increased serum and urinary fructose concentrations in diabetic patients with ketoacidosis or ketosis. Acta Diabetol. **49**, 119-123

37. Craik, J.D. and Elliott, K.R. (1980) Transport of d-fructose and d-galactose into isolated rat hepatocytes. Biochem. J. **192**, 373-375
38. Morrison, A.D., Clements, R.S. and Jr., Winegrad, A.I. (1972) Effects of elevated glucose concentrations on the metabolism of the aortic wall. J. Clin. Invest. **51**, 3114-3123
39. Brownlee, M. (2001) Biochemistry and molecular cell biology of diabetic complications. Nature **414**, 813-820
40. Cox, T.M. (1994) Aldolase b and fructose intolerance. FASEB J. **8**, 62-71
41. Ramasamy, R., Yan, S.F. and Schmidt, A.M. (2006) Methylglyoxal comes of age. Cell **124**, 258-260
42. Guo, Q., Mori, T., Jiang, Y., Hu, C., Osaki, Y., Yoneki, Y., Sun, Y., Hosoya, T., Kawamata, A., Ogawa, S. et al. (2009) Methylglyoxal contributes to the development of insulin resistance and salt sensitivity in sprague-dawley rats. J. Hypertens. **27**, 1664-1671
43. Wu, L. (2006) Is methylglyoxal a causative factor for hypertension development? Can. J. Physiol. Pharmacol. **84**, 129-139
44. Beisswenger, P.J., Howell, S.K., Touchette, A.D., Lal, S. and Szwergold, B.S. (1999) Metformin reduces systemic methylglyoxal levels in type 2 diabetes. Diabetes **48**, 198-202
45. Dhar, A., Dhar, I., Desai, K.M. and Wu, L. (2010) Methylglyoxal scavengers attenuate endothelial dysfunction induced by methylglyoxal and high concentrations of glucose. Br. J. Pharmacol. **161**, 1843-1856
46. Wang, X., Desai, K., Clausen, J.T. and Wu, L. (2004) Increased methylglyoxal and advanced glycation end products in kidney from spontaneously hypertensive rats. Kidney Int. **66**, 2315-2321
47. Wang, X., Chang, T., Jiang, B., Desai, K. and Wu, L. (2007) Attenuation of hypertension development by aminoguanidine in spontaneously hypertensive rats: Role of methylglyoxal. Am. J. Hypertens. **20**, 629-636
48. Wu, L. (2005) The pro-oxidant role of methylglyoxal in mesenteric artery smooth muscle cells. Can. J. Physiol Pharm. **83**, 63-68
49. Mellor, K.M., Bell, J.R., Young, M.J., Ritchie, R.H. and Delbridge, L.M. (2011) Myocardial autophagy activation and suppressed survival signaling is associated with insulin resistance in fructose-fed mice. J. Mol. Cell Cardiol. **50**, 1035-1043
50. Mackenzie, I.S., Wilkinson, I.B. and Cockcroft, J.R. (2002) Assessment of arterial stiffness in clinical practice. QJM **95**, 67-74

51. Hornum, M., Larsen, S., Olsen, O. and Pedersen, J.F. (2006) Duplex ultrasound of the superior mesenteric artery in chronic pancreatitis. Br. J. Radiol. **79**, 804-807
52. Iizuka, K. and Horikawa, Y. (2008) Chrebp: A glucose-activated transcription factor involved in the development of metabolic syndrome. Endocr. J. **55**, 617-624
53. Letexier, D., Peroni, O., Pinteur, C. and Beylot, M. (2005) In vivo expression of carbohydrate responsive element binding protein in lean and obese rats. Diabetes Metab. **31**, 558-566
54. Koo, H.Y., Wallig, M.A., Chung, B.H., Nara, T.Y., Cho, B.H. and Nakamura, M.T. (2008) Dietary fructose induces a wide range of genes with distinct shift in carbohydrate and lipid metabolism in fed and fasted rat liver. Biochim. Biophys. Acta **1782**, 341-348
55. Chang, T., Wang, R., Olson, D.J., Mousseau, D.D., Ross, A.R. and Wu, L. (2011) Modification of akt1 by methylglyoxal promotes the proliferation of vascular smooth muscle cells. FASEB J. **25**, 1746-1757
56. Al-Salami, H., Mamo, J.C., Mooranian, A., Negrulj, R., Lam, V., Elahy, M., Takechi, R. (2016) Long-term supplementation of microencapsulated ursodeoxycholic acid prevents hypertension in a mouse model of insulin resistance. Exp. Clin. Endocrinol. Diabetes May 24. [Epub ahead of print]

Figure legends

Figure 1. The correlation of MG/fructose levels with blood pressures in diabetic patients. (**A)** Serum levels of MG of diabetic patients (*n*=70) and healthy volunteers (*n*=26). (**B)** Positive correlation of serum MG levels with blood pressures. **P*<0.05 *vs*. healthy volunteers; $^{\#}$*P*<0.05 *vs*. diabetic patients with normal blood pressure. The classification of blood pressure levels (mmHg): Normal, <129 (SBP) and <84 (DBP); High normal, 130–139 (SBP) and/or 85–89 (DBP); Grade 1: 140–159 (SBP) and/or 90–99 (DBP); Grade 2: 160–179 (SBP) and/or DBP (100–109). (**C)** Positive correlation of serum MG levels with blood pressures. (**D)** Positive correlation of serum fructose levels with blood pressures. (**E**) Positive correlation of serum fructose levels with MG levels. (F) Relative risk for patients with hypertension by binary logistic regression analysis. Data are odds ratios (ORs) with 95% confidence interval (CI).

Figure 2. Echo ultrasonographic analysis of vascular remodeling in high fructose (Fru, 60%) or control diet (CT)-fed mice. (**A)** Representative ultrasonographic images of blood vessels. (**a**) Images taken at the B mode. The arrows point to where Doppler sample volume is positioned. (**b**) Doppler flow velocity waveforms. The end-diastolic velocity (EDV, left) and the peak systolic velocity (PSV, right) are indicated by the blue lines. (**c**) Images taken at the M mode. The end-diastolic (left) and peak systolic (right) vascular diameters and arterial wall thickness are indicated by the blue lines. (**B**) Summaries of the changes in vascular structure and functions from the ultrasonographic images. *n*=5−8 per group; **P*<0.05 *vs*. CT. CA, left common carotid artery; AA, abdominal aorta; MA, superior mesenteric artery.

Figure 3. Smooth muscle cell hyperplasia in mouse blood vessel walls. (**A**) Representative H&E staining and α-SM actin immunostaining of blood vessels from control (CT) or high fructose (Fru)-fed mice. Magnifications are indicated in each set of panels. (**B**) Quantitative comparisons of the number of VSMCs in blood vessel walls between CT and Fru-fed mice. (**C**) The vessel wall thickness. Each data point represents at least 18 photomicroscope images (400 × magnification) from six animals. **P*<0.05 *vs*. CT. CA, left common carotid artery; AA, abdominal aorta; MA, superior mesenteric artery.

Figure 4. Upregulation of AldoB, ChREBP, Akt1, and FoxO1/3α expression in the aortae of fructose-fed and control (CT) mice. (**A**) AldoA/B mRNA expression in aortic tissues. (**B)** AldoA/B protein levels. (**C**) ChREBP protein levels. (**D**) Phosphorylated and total FoxO1/3α

protein levels. (**E**) Phophorulated and total Akt1 protein levels. *n*=4; **P*<0.05 *vs.* control.

Figure 5. The role of AldoB in fructose-induced MG production and VSMC proliferation. (**A**) Knockdown of *AldoA* and *AldoB* gene expression in A-10 cells with respective siRNAs. Typical Western blot results are depicted (upper panel) along with the statistical analysis (lower panel). *n*=4; **P*<0.05. (**B)** MG levels in A-10 cells treated with fructose (10 mM) and/or insulin (100 nM) for 6 h. *n*=4; **P*<0.05 *vs*. CT; $^{\#}$*P*<0.05 *vs*. control siRNA. (**C**) A-10 cell proliferation measured by MTT assays after treatment with fructose and/or insulin for 48 h (*n*=6). CT, control in the absence of any siRNA treatment; Ins, insulin; Fru, fructose; MG, methylglyoxal.

Figure 6. The effects of fructose on intracellular ChREBP apartmentalization and *AldoB* gene activation. (**A**) Western blot analysis of ChREBP in A-10 cells treated with insulin (100 nM) and/or fructose (0.3 or 10 mM) for 6 h (*n*=4). (**B**) Western blots of fractionated cytoplasmic and nuclear lysates from A-10 cells treated with insulin and/or fructose for 6 h. Typical results are depicted in upper panel along with the statistical analysis in lower panel. *n*=4. (**C**) Binding of ChREBP to *AldoB* promoter. After A-10 cells were treated with fructose and/or insulin for 6 h, ChIP was performed using the Epi Tect ChIP One-Day Kit. The cells were sonicated to shear DNA and the sonicated supernatant (input) was immunoprecipitated with non-specific rabbit IgG (the negative control, NC), anti-ChREBP antibodies. The precipitated chromatin DNA was purified and amplified by quantitative PCR using AldoB primers. Representative gel (upper panel) and summary of results expressed as the fold changes over untreated control cells (lower panel. *n*=3. (**D**) Localization of ChREBP and AldoB proteins in aortic tissues from control (CT) or fructose (Fru)-fed mice. Representative images were shown in the upper panel and the quantification of the ratio of cytoplasmic/nuclear fluorescence intensity was shown in lower panel. Scale bar, 100 μm. **P*<0.05 *vs*. CT.

Figure 7. Fructose regulates AldoB expression via ChREBP activation. (**A**) Western blot analysis of ChREBP protein levels. A-10 cells transfected with ChREBP-siRNA were treated with insulin (100 nM) and/or fructose (10 mM) for 6 h prior to Western blot analysis. Typical results are depicted in upper panel along with the statistical analysis in lower panel. *n*=4. (**B**) A-10 cell MG levels. *n*=4. (**C**) The proliferation of A-10 cells transfected with ChREBP-siRNA and treated with insulin (100 nM) and/or fructose (10 mM) for 48 h. Cell proliferation was measured by MTT assays. *n*=6. **P* < 0.05 *vs.* CT (without any siRNA treatment); $^{\#}$*P* < 0.05 *vs.* control siRNA.

Figure 8. The effects of fructose on intracellular apartmentalization of FoxO1/3α and their binding to the DNA-binding element in *AldoB* promoter region. (**A**) Western blot analysis of the cytoplasmic and nuclear lysates of A-10 cells treated with 100 nM insulin and/or 0.3 or 10 mM fructose for 6 h. Typical results are depicted in upper panel along with the statistical analysis in lower panel. *n*=4. (**B**) Binding of FoxO1/3α to *Aldo B* promoter in A-10 cells after fructose and/or insulin treatment for 6 h. The sonicated supernatant (input) were immunoprecipitated with nonspecific rabbit IgG (NC), anti-FoxO1/3α antibodies. Representative gels were shown in the upper panel and the summary of results was shown in lower panel. *n*=3. (**C**) The interaction of fructose and FoxO1 on AldoB expression. A-10 cells transfected with FoxO1-siRNA were treated with 100 nM insulin and/or 10 mM fructose for 6 h prior to Western blot analysis. Typical results are depicted in upper panel along with the statistical analysis in lower panel. *n*=4. (**D**) The interaction of fructose and FoxO3α on AldoB expression. *n*=4. **P*<0.05 *vs.* CT (without any siRNA treatment); $^{\#}P$<0.05 *vs.* control siRNA.

Figure 1

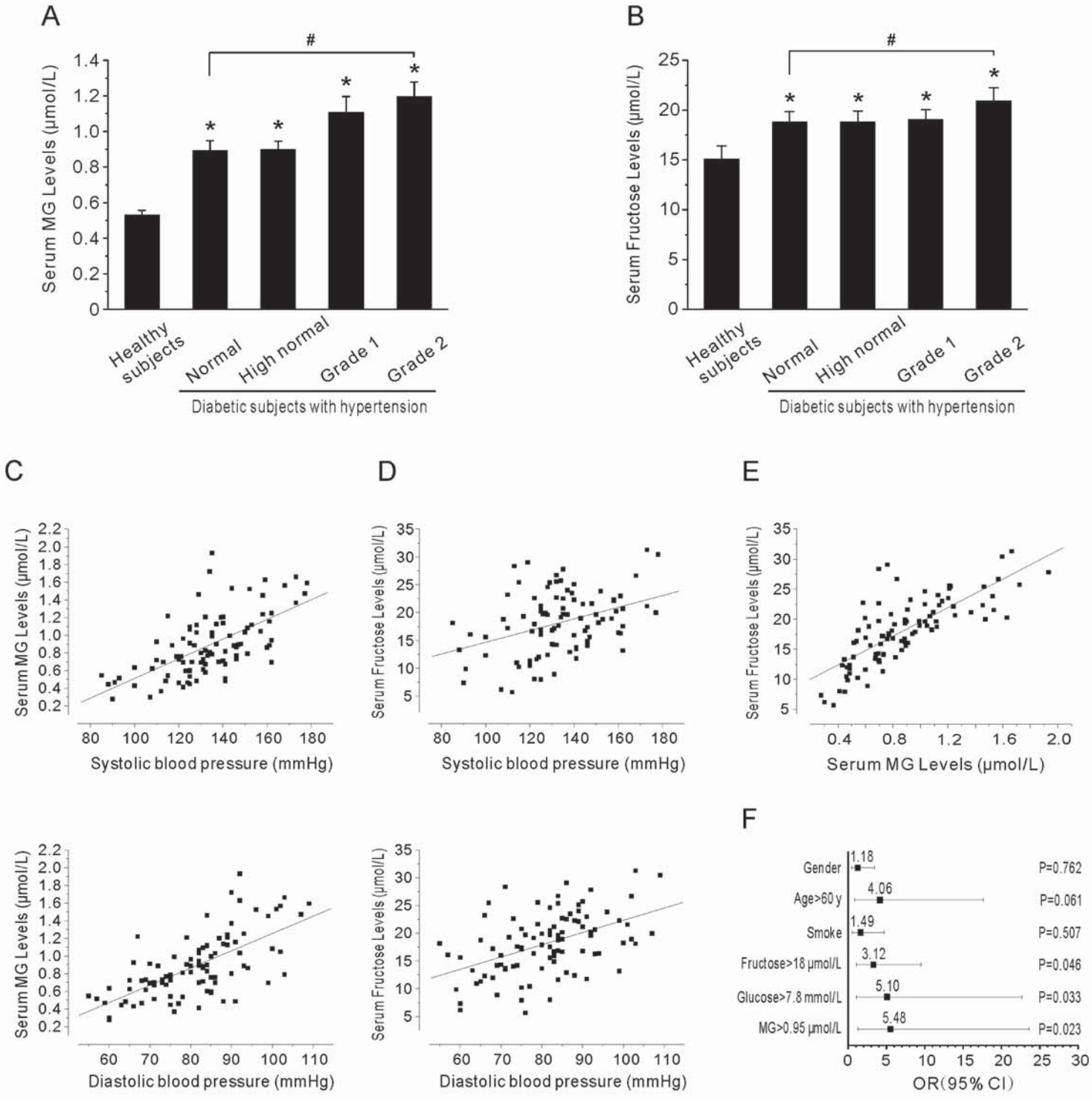
A
Serum MG Levels (μmol/L)
Healthy subjects
Normal
High normal
Grade 1
Grade 2
Diabetic subjects with hypertension
B
Serum Fructose Levels (μmol/L)
C
Systolic blood pressure (mmHg)
Diastolic blood pressure (mmHg)
D
E
Serum MG Levels (μmol/L)
F
Gender
Age>60 y
Smoke
Fructose>18 μmol/L
Glucose>7.8 mmol/L
MG>0.95 μmol/L
P=0.762
P=0.061
P=0.507
P=0.046
P=0.033
P=0.023
OR(95% CI)

Figure 2

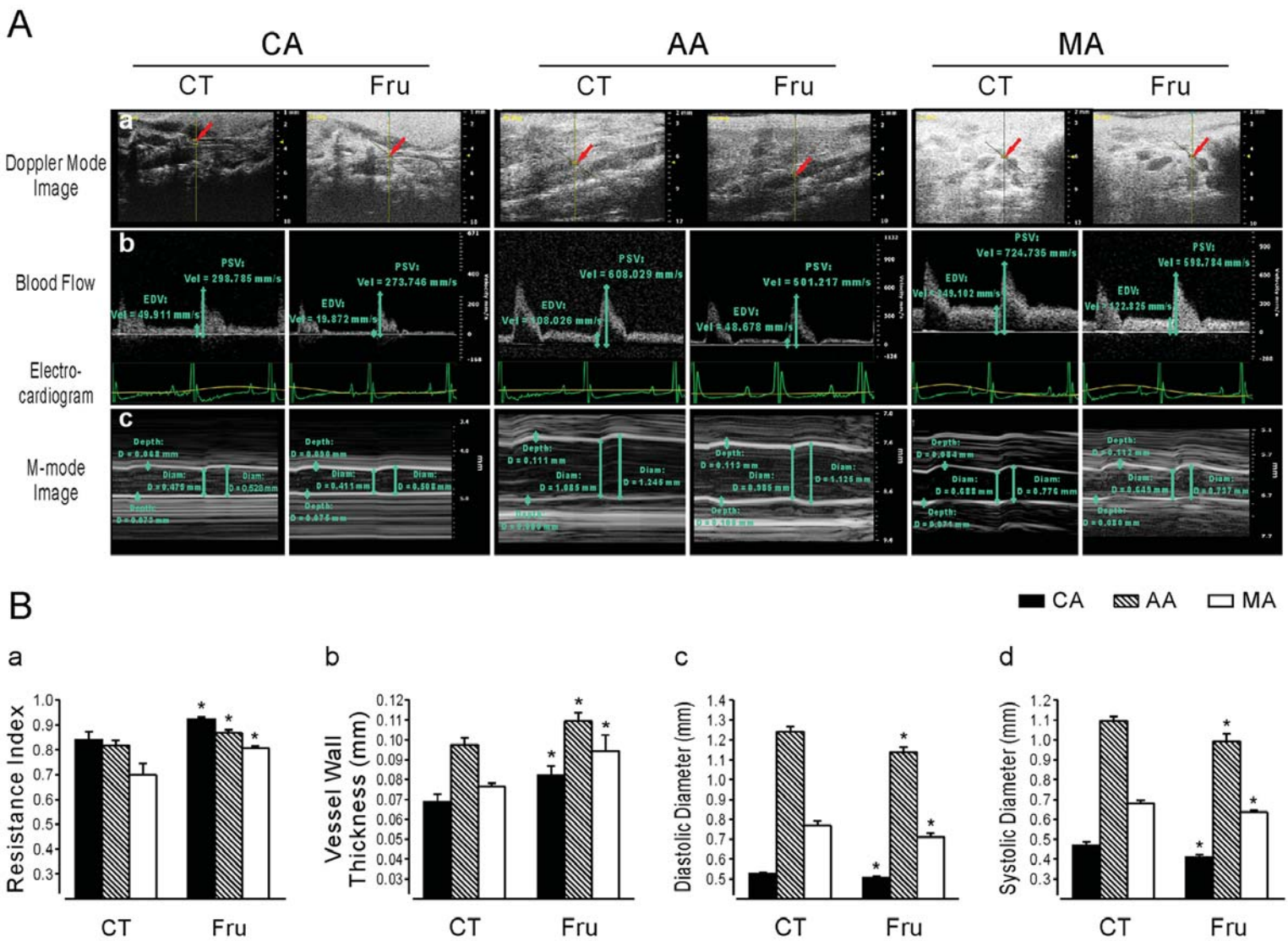
A
CA
AA
MA
CT
Fru
CT
Fru
CT
Fru
Doppler Mode Image
Blood Flow
Electro-cardiogram
M-mode Image
a
b
c
PSV:
Vel = 298.785 mm/s
EDV:
Vel = 49.911 mm/s
PSV:
Vel = 273.746 mm/s
EDV:
Vel = 19.872 mm/s
PSV:
Vel = 608.029 mm/s
EDV:
Vel = 108.026 mm/s
PSV:
Vel = 501.217 mm/s
EDV:
Vel = 48.678 mm/s
PSV:
Vel = 724.735 mm/s
EDV:
Vel = 149.102 mm/s
PSV:
Vel = 598.784 mm/s
EDV:
Vel = 122.825 mm/s
Depth:
D = 0.111 mm
Diam:
D = 1.085 mm
Diam:
D = 1.345 mm
Depth:
D = 0.113 mm
Diam:
D = 0.985 mm
Diam:
D = 1.126 mm
Diam:
D = 0.776 mm
Diam:
D = 0.737 mm

B
CA
AA
MA
a
b
c
d
Resistance Index
Vessel Wall Thickness (mm)
Diastolic Diameter (mm)
Systolic Diameter (mm)
CT
Fru

Figure 3

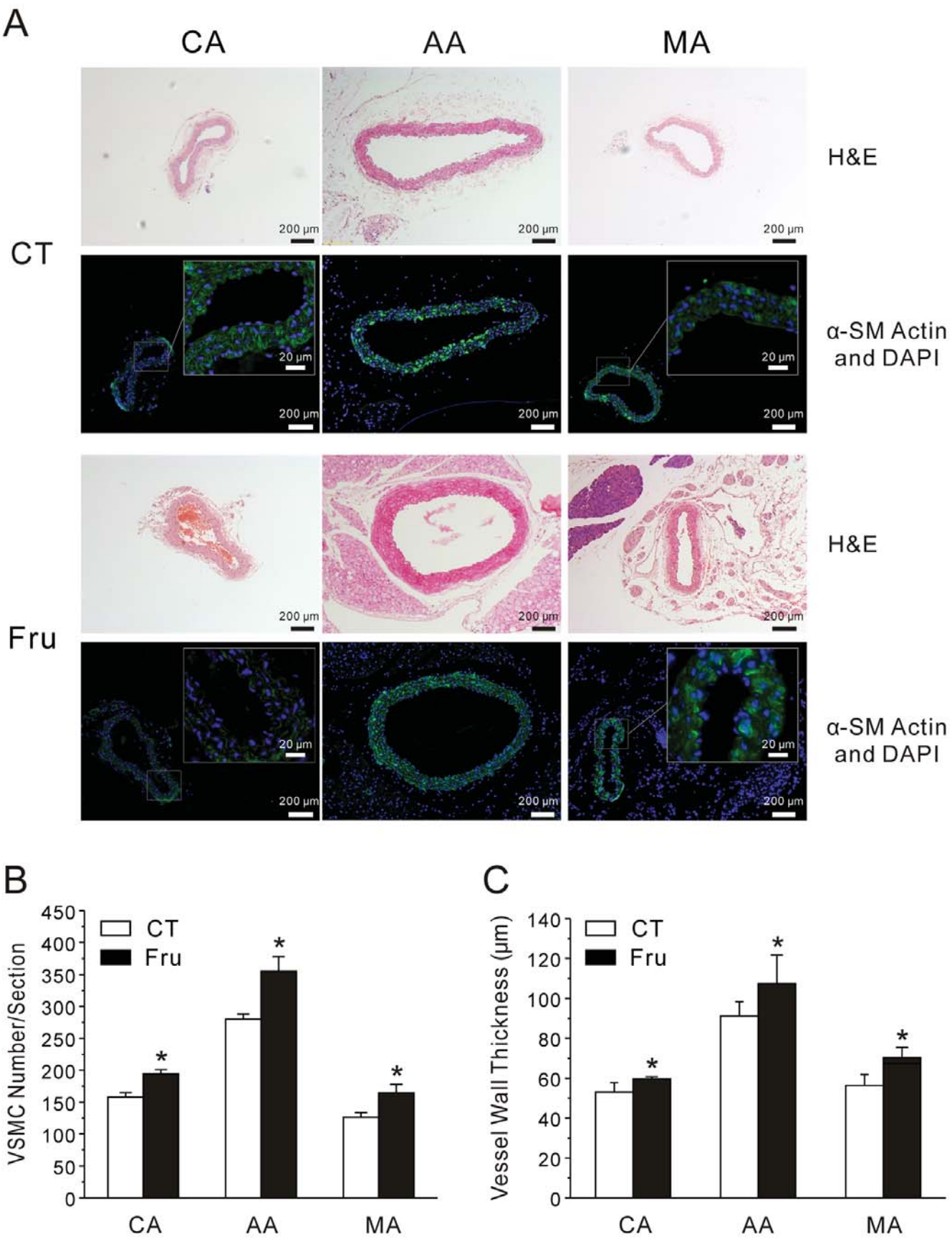
A
CA
AA
MA
H&E
CT
α-SM Actin and DAPI
H&E
Fru
α-SM Actin and DAPI
200 μm
20 μm
B
VSMC Number/Section
CT
Fru
CA
AA
MA
C
Vessel Wall Thickness (μm)
CT
Fru
CA
AA
MA

Figure 4

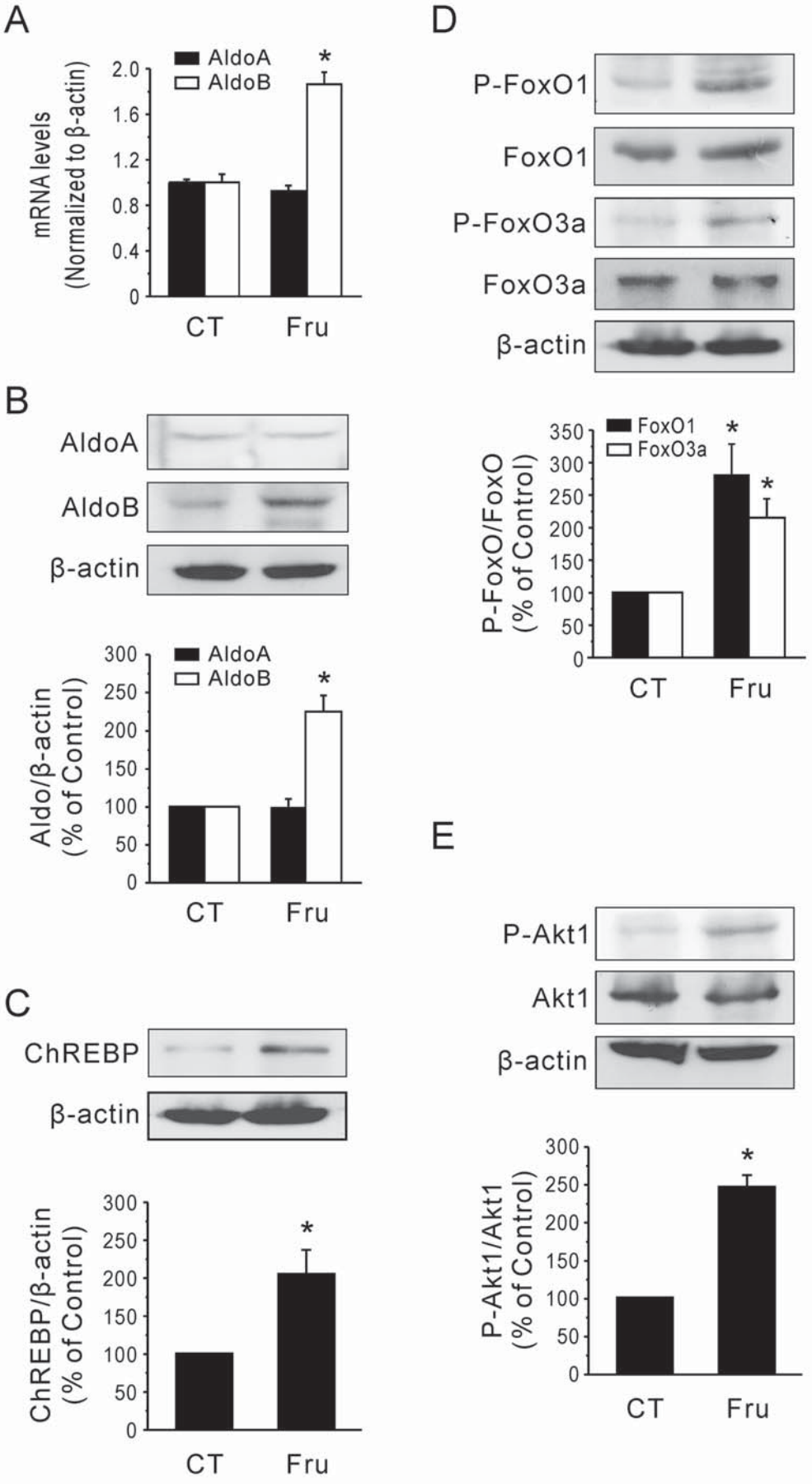
A
AldoA
AldoB
*
mRNA levels
(Normalized to β-actin)
2.0
1.6
1.2
0.8
0.4
0
CT
Fru
B
AldoA
AldoB
β-actin
AldoA
AldoB
*
Aldo/β-actin
(% of Control)
300
250
200
150
100
50
0
CT
Fru
C
ChREBP
β-actin
*
ChREBP/β-actin
(% of Control)
300
250
200
150
100
50
0
CT
Fru
D
P-FoxO1
FoxO1
P-FoxO3a
FoxO3a
β-actin
FoxO1
FoxO3a
*
*
P-FoxO/FoxO
(% of Control)
350
300
250
200
150
100
50
0
CT
Fru
E
P-Akt1
Akt1
β-actin
*
P-Akt1/Akt1
(% of Control)
300
250
200
150
100
50
0
CT
Fru

Figure 5

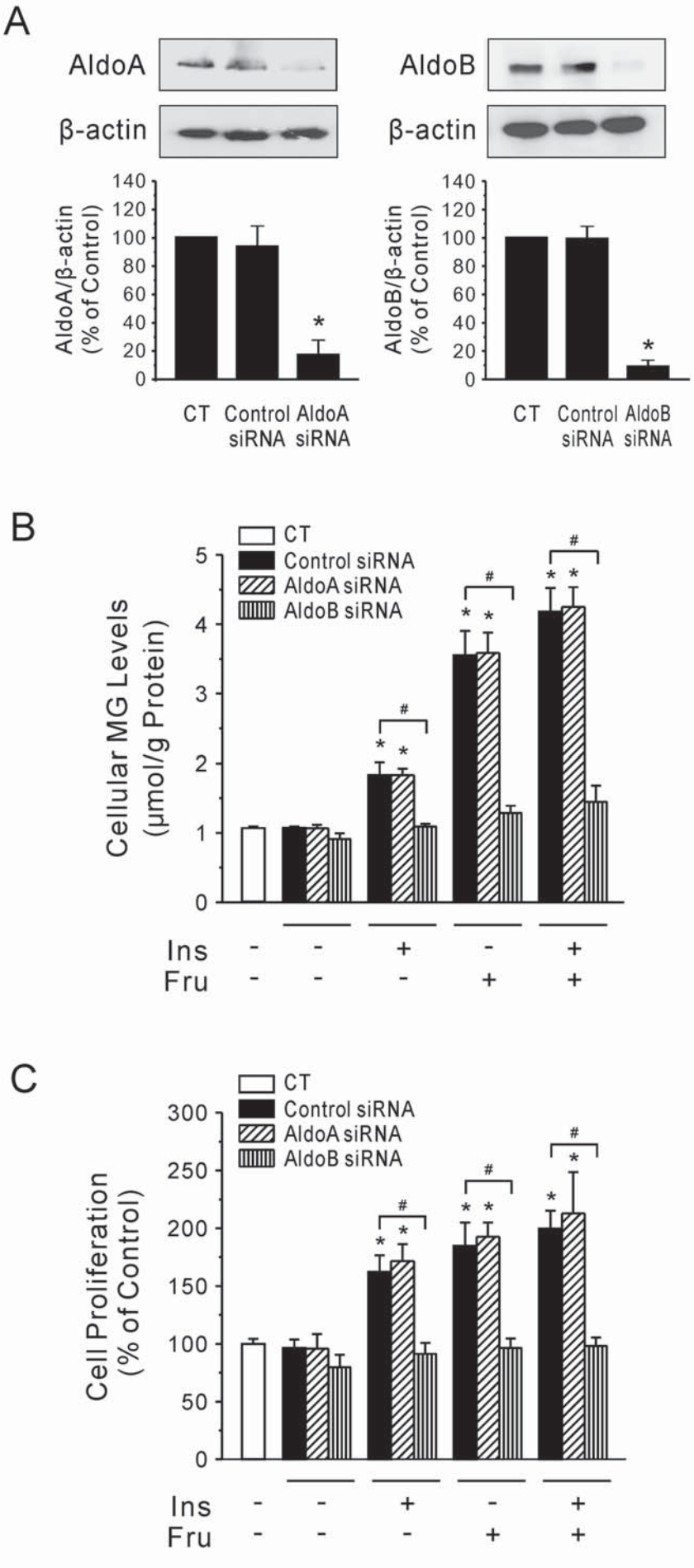
A
AldoA
β-actin
AldoB
β-actin
AldoA/β-actin (% of Control)
AldoB/β-actin (% of Control)
140
120
100
80
60
40
20
0
*
CT
Control siRNA
AldoA siRNA
AldoB siRNA
B
Cellular MG Levels (μmol/g Protein)
CT
Control siRNA
AldoA siRNA
AldoB siRNA
5
4
3
2
1
0
*
#
Ins - - + - +
Fru - - - + +
C
Cell Proliferation (% of Control)
300
250
200
150
100
50
0
Ins - - + - +
Fru - - - + +

Figure 6

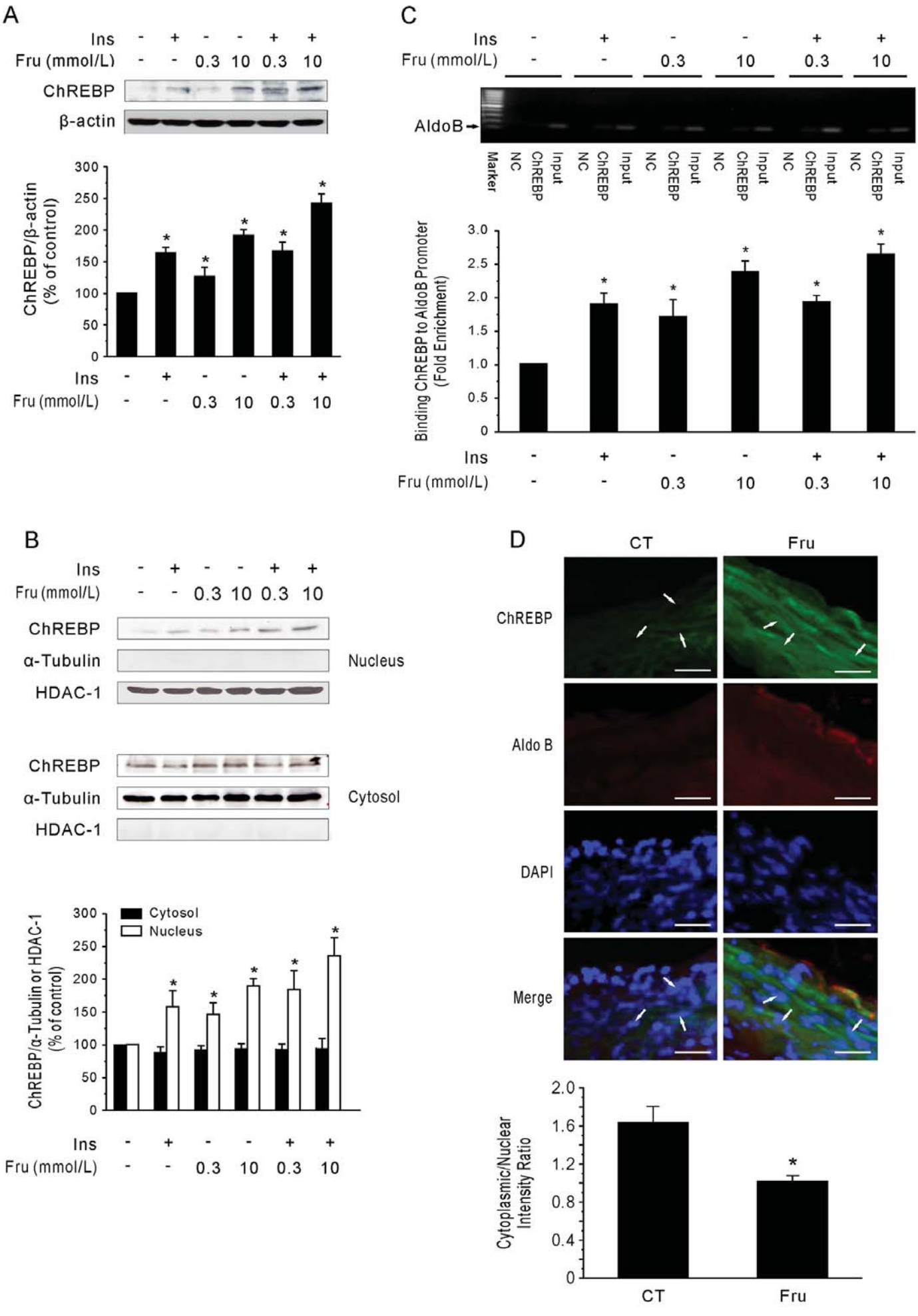
A
Ins - + - - + +
Fru (mmol/L) - - 0.3 10 0.3 10
ChREBP
β-actin
ChREBP/β-actin (% of control)
300
250
200
150
100
50
0
Ins - + - - + +
Fru (mmol/L) - - 0.3 10 0.3 10
C
Ins - + - - + +
Fru (mmol/L) - - 0.3 10 0.3 10
AldoB
Marker
NC
ChREBP
Input
Binding ChREBP to AldoB Promoter (Fold Enrichment)
3.0
2.5
2.0
1.5
1.0
0.5
0
Ins - + - - + +
Fru (mmol/L) - - 0.3 10 0.3 10
B
Ins - + - - + +
Fru (mmol/L) - - 0.3 10 0.3 10
ChREBP
α-Tubulin
HDAC-1
Nucleus
ChREBP
α-Tubulin
HDAC-1
Cytosol
ChREBP/α-Tubulin or HDAC-1 (% of control)
Cytosol
Nucleus
300
250
200
150
100
50
0
Ins - + - - + +
Fru (mmol/L) - - 0.3 10 0.3 10
D
CT
Fru
ChREBP
Aldo B
DAPI
Merge
Cytoplasmic/Nuclear Intensity Ratio
2.0
1.6
1.2
0.8
0.4
0
CT
Fru

Figure 7

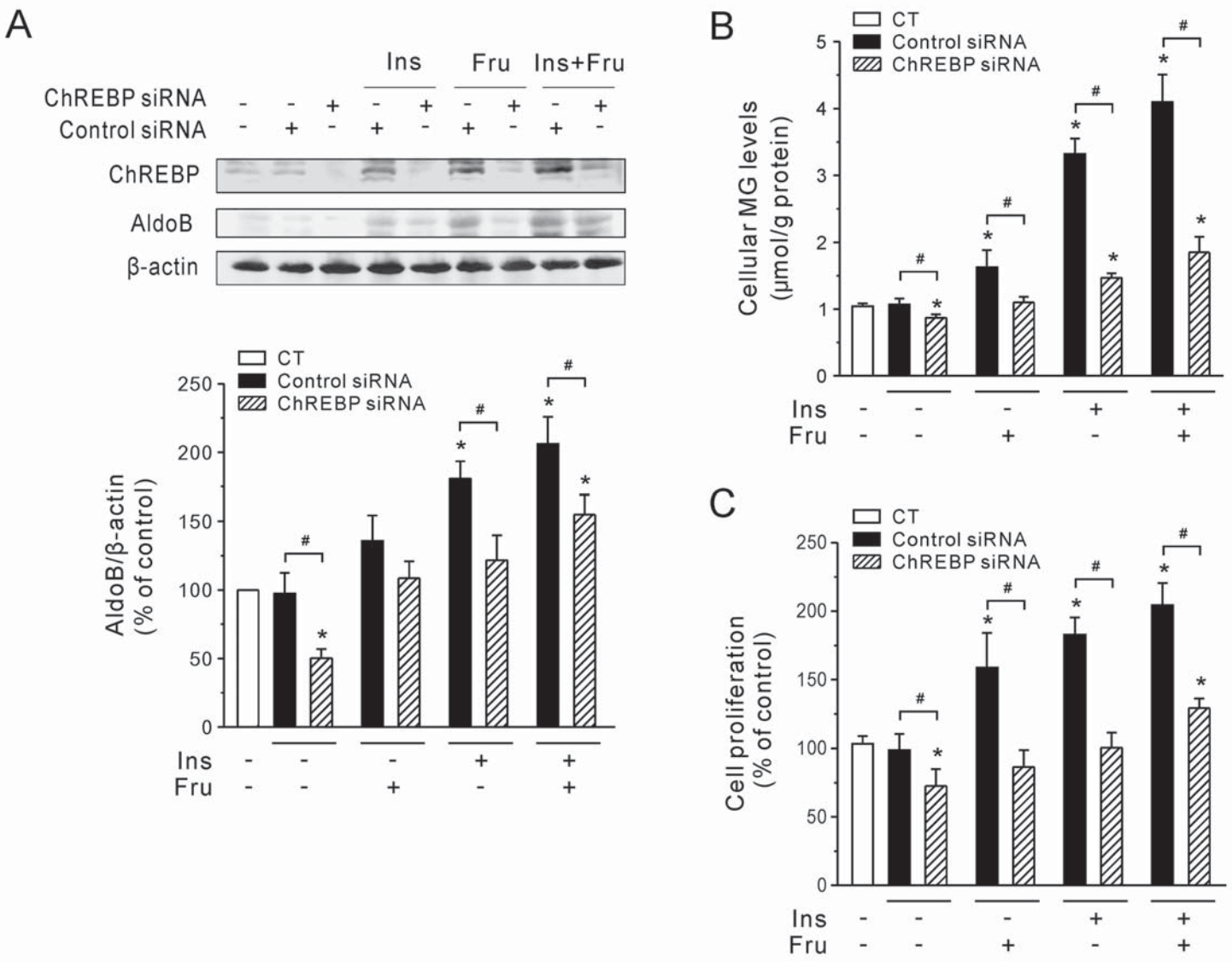
A
Ins
Fru
Ins+Fru
ChREBP siRNA
Control siRNA
ChREBP
AldoB
β-actin
CT
Control siRNA
ChREBP siRNA
AldoB/β-actin
(% of control)
Ins
Fru
B
Cellular MG levels
(μmol/g protein)
C
Cell proliferation
(% of control)

Figure 8

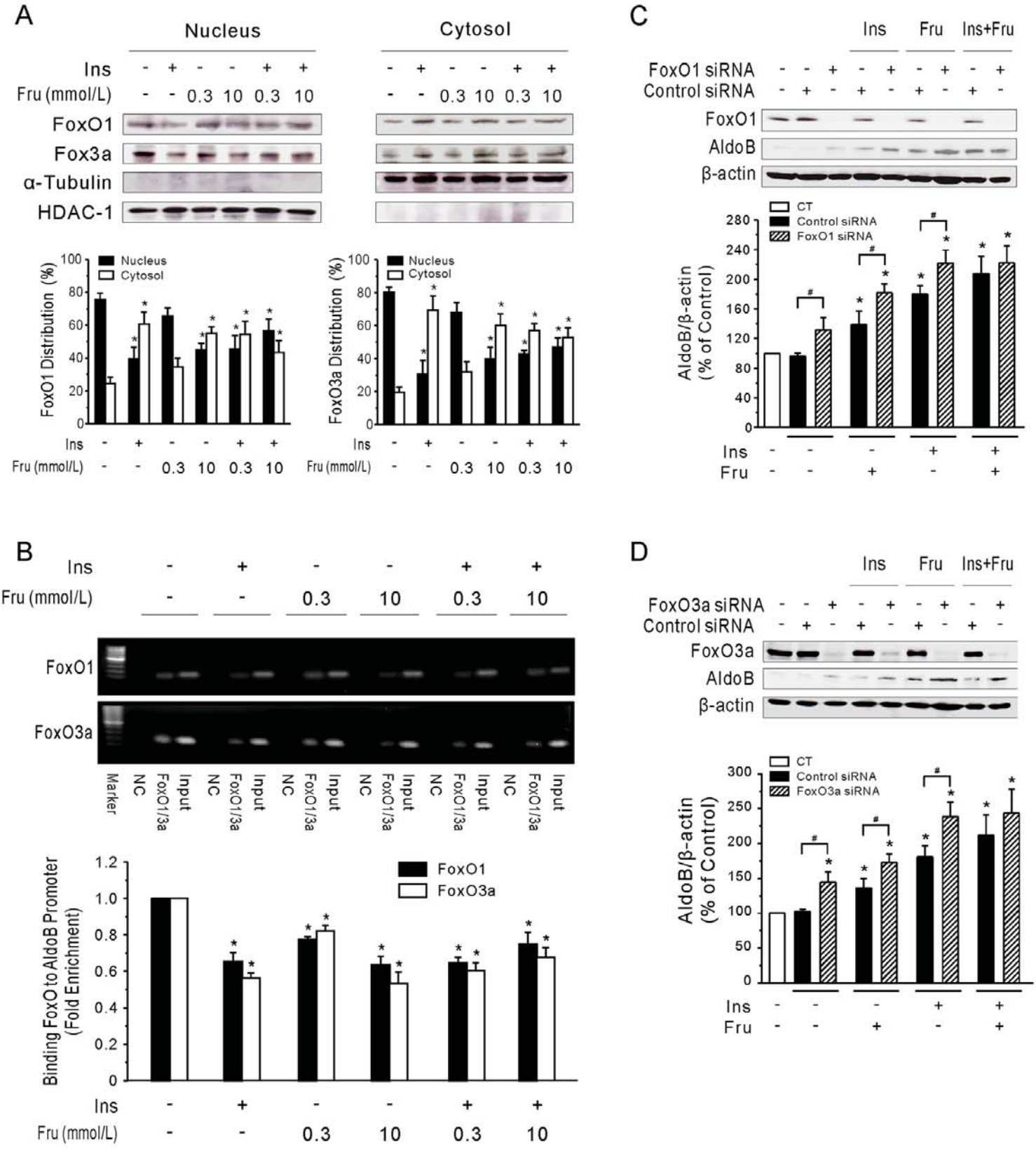
A
Nucleus
Cytosol
Ins
Fru (mmol/L)
FoxO1
Fox3a
α-Tubulin
HDAC-1
FoxO1 Distribution (%)
FoxO3a Distribution (%)
Nucleus
Cytosol
B
Ins
Fru (mmol/L)
FoxO1
FoxO3a
Marker
NC
FoxO1/3a
Input
Binding FoxO to AldoB Promoter (Fold Enrichment)
FoxO1
FoxO3a
C
Ins
Fru
Ins+Fru
FoxO1 siRNA
Control siRNA
FoxO1
AldoB
β-actin
CT
Control siRNA
FoxO1 siRNA
AldoB/β-actin (% of Control)
D
FoxO3a siRNA
Control siRNA
FoxO3a
AldoB
β-actin
CT
Control siRNA
FoxO3a siRNA
AldoB/β-actin (% of Control)